VNU Journal of Science: Mathematics – Physics, Vol. 39, No. 4 (2023) 71-79

VNU Journal of Science: Mathematics - Physics

Journal homepage: https://js.vnu.edu.vn/MaP

Original Article

Influence of Doping Zn on H_2 Sensing Characteristics of Nickel Ferrite Nanoparticles

Dao Thi Thuy Nguyet, Nguyen Phuc Duong, Luong Ngoc Anh*

International Training Institute for Material of Science (ITIMS)
Hanoi University of Science and Technology (HUST), 1 Dai Co Viet, Hai Ba Trung, Hanoi, Vietnam

Received 24 April 2023
Revised 06 July 2023; Accepted 10 July 2023

Abstract: In this work, H_2 gas sensors were prepared using nickel zinc ferrite $NiFe_2O_4$ and $Ni_{0.5}Zn_{0.5}Fe_2O_4$ nanoparticles, then the hydrogen gas sensing performance of the sensors was tested. The nickel zinc ferrite nanoparticles were synthesized by chemical co-precipitation combined with thermal annealing. Crystalline Structure and morphology characterization of synthesized powders was made by using X-ray diffraction (XRD) and Transmission electron microscopy (TEM) analysis, respectively. Nano powder resulting from milling was used to prepare gas sensing elements in pellet form. The gas-sensing properties were studied in the presence of hydrogen as test gases. The gas response was found to be strongly influenced by the Zn substitution doping concentration in $NiFe_2O_4$. A significant high sensitivity of ~ 90% was found for the compound of $Ni_{0.5}Zn_{0.5}Fe_2O_4$. in the presence of 500 ppm H_2 at the operating temperature of 250 °C.

Keywords: Nickel zinc ferrite, H_2 sensing, gas properties, nanoparticles, co-precipitation.

1. Introduction

Ferrite materials have numerous advantages for gas sensing applications. They exhibit high chemical stability, excellent mechanical resistance and are less susceptible to temperature variations when compared to conventional materials used in gas sensing devices [1-8]. Nickel ferrite is of interest for research gas sensing because of their special properties at the nanometer scale such as quantum effects, surface effects, easy doping other metals, etc. [9-16]. The sensitivities of the electrical resistivity to acetone, ethanol, methane (CH_4), and liquefied petroleum gas (LPG) of nickel ferrite doped with small

* Corresponding author.
E-mail address: anh.luongngoc@hust.edu.vn

https//doi.org/10.25073/2588-1124/vnumap.4847

amounts of calcium, cobalt, and manganese were investigated [17]. Zohrabi et al. reported on the gas sensing properties of $Ni_{0.6}Zn_{0.4}Fe_2O_4$ nanoparticles, the Ni-Zn ferrite indicated a good response toward the acetone gas compared to the methanol gas, and the best operating temperature for both gases was found to be of 250 °C. In a study by Muraishi et al., [18], nickel ferrite sensors have been extensively studied, and researchers have found that doping them with rare earth oxides additives such as LaO, SmO, and YO can have significant benefits. By doping these additives one can improve the sensors' sensitivity and shorten their response time significantly. $NiFe_2O_4$ incorporated with Pd is found to be selective for the detection of liquefied petroleum gas at an operating temperature of 200 °C [19]. Reddy et al., [20] found that palladium incorporated into nickel ferrite reduced the temperature of operation and accelerated the response time. The study conducted by Iftimie et al., explores the effect of manganese substitution on the temperature-dependent sensitivity of Ni-Co ferrite [21]. Nanocrystalline nickel ferrite has been found to have a high potential for gas sensing applications due to its outstanding electrical and magnetic properties, as well as its high surface-to-volume ratio. The influence of the matherial's particle size on the H_2 and H_2S sensing characteristics was investigated [22].

Our previous studies examined the gas-sensitivity properties of copper ferrite, specifically in detecting H_2S gas. The results showed a promising application of this material in gas-sensing technologies. In this work we focused on researching properties of ferritic materials and the potential implications of these findings for the development of gas-sensing materials [7, 23].

In this work, we have shown that the addition of Zn to nanocrystalline nickel ferrite enhanced its H_2 sensing properties, such as sensitivity, response time, and stability. This is explained due to the formation of defects and oxygen vacancies in the crystal structure due to the substitution of Zn ions in place of Ni ions. These defects generated more active sites for H_2 gas to interact with, resulting in improved sensing performance.

2. Experimental

Nickel zinc ferrite nanoparticles were synthesized by the chemical co-precipitation method. A homogeneous solution of $FeCl_3.6H_2O$, $ZnCl_2$, and $NiCl_2$ (Sigma Aldrich 99%) in distilled water was prepared in a molar ratio of Ni: Zn: Fe = (1-x): x: 2 (x = 0, 0.5). An ammonium hydroxide solution (Sigma Aldrich 30-33% NH_3 in H_2O) was added to obtain pH =10. Immediately, the solution was heated up to 90 °C for one hour. Precipitation and formation of ferrite phases take place by the conversion of metal salts into hydroxides, which occurs immediately, and is followed by the transformation of hydroxides into ferrites. This duration was necessary to ensure the transformation of hydroxides into spinel ferrite (dehydration and atomic rearrangement involved in the conversion of intermediate hydroxide phase into ferrite). The fine particles were washed several times with distilled water, followed by acetone rinse in a magnetic field. Afterward, they were dried at 60 °C for 12 hours. To stabilize the spinel structure and achieve high crystallinity, a heat treatment process was required for the samples. The samples of different compositions were obtained by annealing as-precipitated products at 600 °C in the air for 5 hours.

The morphologies and microstructures of nickel zinc ferrite nanoparticles samples were observed by a JEOL 1010 transmission electron microscopy (TEM) and a Siemens D-5000 X-ray diffractometer (XRD) using Cu-Kα tube (λ = 1.54056 Å). The synthesized $Ni_{1-x}Zn_xFe_2O_4$ (x = 0, 0.5) nanoparticles were mixed with polyvinyl alcohol and then pressed into pellets (cylindrical discs) of approximately 1 mm thickness and 10 mm diameter at a pressure of 150 MPa. These pellets were heat-treated at 250 °C for 1 hour to burn out organic compounds and facilitate solid-state sintering and then were cooled in the furnace. For gas-sensing measurements, the ferrite pellet was provided with a heater, and the assembled

heater element was introduced in a chamber. The DC electrical resistivity was measured by the two-probe method. High purity silver paint electrodes were applied to either face of the samples for good electrical contacts. The test gases were injected with four mass flow controllers [24]. Sensors were tested in a chamber that allowed temperature control and mass flow control with 100, 250, and 500 ppm H_2/ balance N_2 at 250 °C. The responsibility of the sensor to H_2 was calculated using equation (1) where R_a and R_g is the sensor resistance without and with gas presence, respectively.

$$S = \frac{|R_a - R_g|}{R_a} \quad (1)$$

3. Results and Discussion

The XRD patterns of synthesized nickel zinc ferrite nanoparticles are shown in Fig. 1. This figure indicates that the nanoparticle samples exhibit a completely single-crystalline phase. All the observed diffraction peaks are consistent with the one of the $NiFe_2O_4$ cubic spinel-crystal structure (JCPDS card No. 54-0964). Main diffraction peaks are obtained from orientations of (311), (400), (511), and (440).

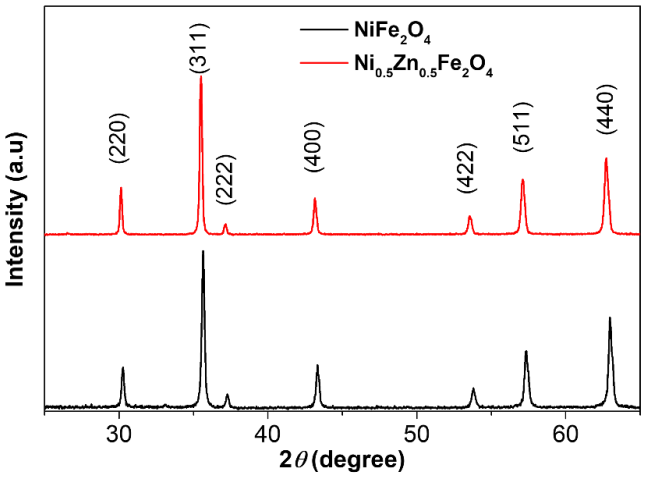

Figure 1. XRD patterns of $NiFe_2O_4$ and $Ni_{0.5}Zn_{0.5}Fe_2O_4$ annealed at 800 ºC/5 h.

The lattice parameter (a) was determined by using Bragg formula, average size of the crystallites were calculated by Debye-Scherrer equation. The data are listed in Table 1.

Table 1. The lattice parameters (a) and the average crystallite size (D_{XRD}), cation distribution (A)[B] in A and B sites [25] of the $NiFe_2O_4$ and $Ni_{0.5}Zn_{0.5}Fe_2O_4$ samples annealed at 800 °C/5 h.

Sample	$NiFe_2O_4$	$Ni_{0.5}Zn_{0.5}Fe_2O_4$
Lattice parameter, (Å)	a = 8.3215	a = 8.3623
Cation distribution (A)[B] [25]	$(Fe)_A$ $[NiFe]_B$	$(Zn_{0.5}Fe_{0.5})_A$ $[Ni_{0.5}Fe_{1.5}]_B$
The average crystallite (D_{XRD}), nm	31	33

Most intuitively, a shift of the diffraction peak can be observed to the left when the Zn^{2+} ion is substituted in Ni^{2+}. The lattice parameter increases almost linearly with increasing Zn^{2+} content. According to the Rietveld calculations, Zn ions occupy both tetrahedral and octahedral sublattices [25]. Its ionic radius is much greater than the ionic radii of Ni^{2+} and Fe^{3+} ions (r_{Zn} = 0.74 Å, r_{Fe}= 0.63 Å, r_{Ni} = 0.69 Å for the tetragonal site and r_{Zn} = 0.9 Å, r_{Fe} = 0.785 Å, r_{Ni} = 0.83 Å for the octahedral site) [26]. Zinc doping can lead to an increase in the lattice constant of the sample, which is the distance between the atoms in the crystal. This happens because zinc ions are larger than the original host atoms in the crystal structure, and therefore, the lattice needs to expand to accommodate the larger ions. As the concentration of zinc doping increases, the number of larger ions in the crystal increases, leading to a greater expansion of the lattice constant. This can result in important effects on the properties of the material, such as changes in conductivity and optical properties. The average grain sizes (D_{XRD}) of $NiFe_2O_4$ and $Ni_{0.5}Zn_{0.5}Fe_2O_4$ nanoparticles are estimated to be 30 nm, respectively. Whereas, by TEM images one can see that the size of the separated nanoparticles as shown in Fig. 2 hasa size in the range of 20-60 nm with spherical and elongated particles-like morphology. From the TEM images, both nanoparticle samples have unevenly distributed particle sizes with similar. The particles are spherical and clustered together. A slight increase in lattice parameters was noted which can be attributable to Zn doping (Table 1).

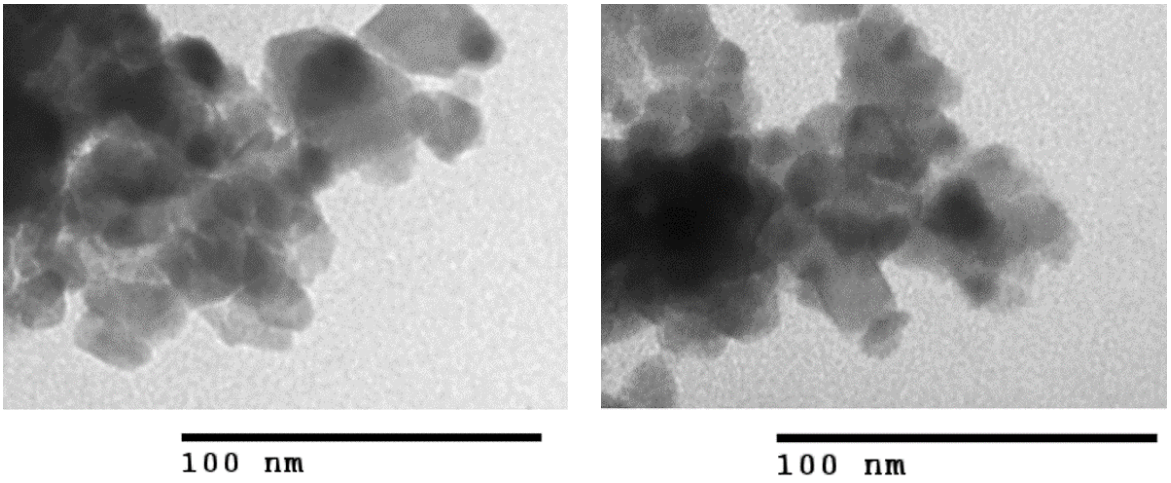

Figure 2. TEM images of $NiFe_2O_4$ (left) and $Ni_{0.5}Zn_{0.5}Fe_2O_4$ (right) annealed at 800 ºC/5 h.

Figs. 3a and 3b illustrate the sensing transients of the nickel ferrite sensor for 50, 100, and 500 ppm H_2 at 250 °C. The initial resistances of $NiFe_2O_4$ and $Ni_{0.5}Zn_{0.5}Fe_2O_4$ nanoparticles at 250 °C measured in the air were approximate 50 MΩ and 1.5 GΩ, respectively. The initial resistance of the $Ni_{0.5}Zn_{0.5}Fe_2O_4$ sample was larger than that of the $NiFe_2O_4$ sample. This possibly caused by the doping of Zn, resulting in the formation of poor conducting regions between two sublattice sites (tetrahedral and octahedral site). The change in the electrical resistance of $Ni_{0.5}Zn_{0.5}Fe_2O_4$ nanoparticles when exposed to different H_2 concentrations can appear as a trend like that of sample $NiFe_2O_4$. However, the resistance of the $Ni_{0.5}Zn_{0.5}Fe_2O_4$ sample vs. H_2 concentration is significantly reduced than that of the $NiFe_2O_4$ sample, indicating a higher sensitivity of the $Ni_{0.5}Zn_{0.5}Fe_2O_4$ nanoparticles. In addition, the response time of the Zn-substituted sample is also improved by about 25 seconds compared to 50 seconds for the pure sample. Further comparisons of the H_2 sensor properties were conducted. The sensing response of pure and Zn-doped samples as a function of H_2 concentration ranges from 100 ppm

to 500 ppm (Fig. 3). The operating mechanism of the spinel ferrite gas sensor is like that of a semiconductor gas sensor. Oxygen species chemisorb onto metal oxide particles, thereby trapping electrons. This chemisorption produces a resistance layer from an electron-depleted space charge on the *n*-type particle surface or conducting layer from accumulated holes on the *p*-type particle. Electrons are released from oxygen back to oxide when the gas molecules react with chemisorbed oxygen. The release of electrons changes the conductivity in the space-charge layer. In spinel ferrite, the sensing mechanism is based on a surface-controlled process. This involves the adsorption and ionization of oxygen from the air, which contains the test gas analyte (Eqs. 2- 7). The interaction between hydrogen molecules and the ferrite structure is crucial for its sensing ability. When hydrogen gas comes into contact with the nickel ferrite surface, it diffuses into the crystal structure, creating defects and altering the electrical properties of the material. Consequently, the resistance of the ferrite material changes, allowing for the measurement and correlation of hydrogen gas concentration. The unique composition of nickel zinc ferrite, with the presence of nickel and zinc ions, enhances the adsorption of hydrogen on the surface, thereby increasing the material's sensitivity.

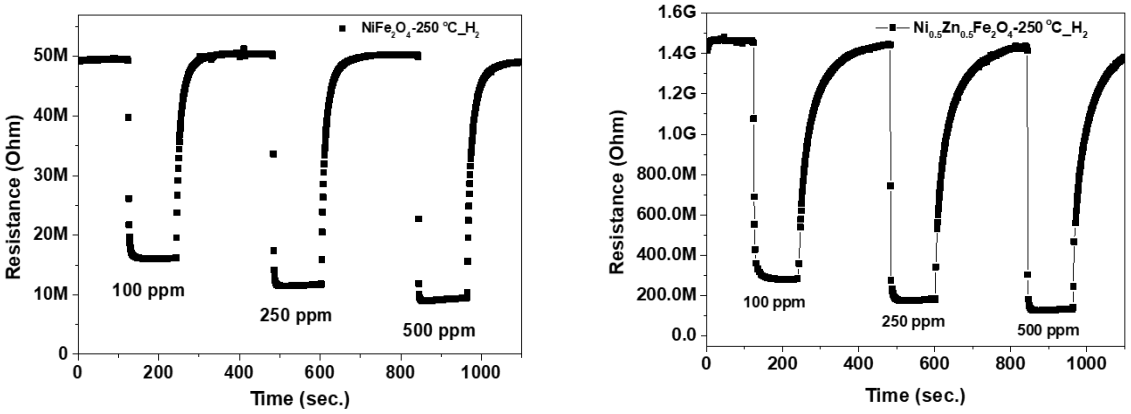

(a) (b)

Figure 3. Transient resistance vs. time upon exposure to different H_2 concentrations at 250 °C for the pure (a) and Zn-doped $NiFe_2O_4$ (b).

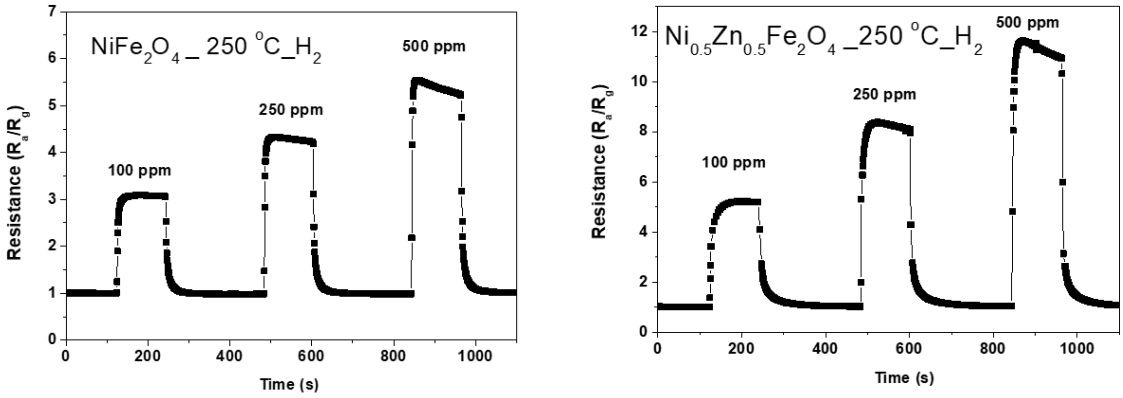

(a) (b)

Figure 4. Transient resistance vs. time upon exposure to different H_2 concentrations of $NiFe_2O_4$ (a) and $Ni_{0.5}Zn_{0.5}Fe_2O_4$ (b).

The sensing response (R_a/R_g) to H_2 gas of the $NiFe_2O_4$ and $Ni_{0.5}Zn_{0.5}Fe_2O_4$ nanoparticles were measured at 250 °C (Fig. 4). The enhancement of the sensitivity with increasing Zn concentration is attributed to the increase of oxygen species concentration on the surface by replacing adsorbed hydroxyl groups and conversion of adsorbed oxygen species into negatively charged chemisorbed species (O_2^-, O^- or O^{2-} depending on temperature), thus attracting more electrons from the samples [27-29]. The *p*-type semiconducting characteristics of the $NiFe_2O_4$ caused by vacancies occur in cation sites, where each cation vacancy, two Ni^{2+} at lattice sites are oxidized to Ni^{3+} to keep the electrical neutrality, hence there must be two holes formed from each metal vacancy.

During gas sensing measurement, the oxygen molecules in air absorb on the surface of $NiFe_2O_4$ (Eqs. (2) – (5)) and withdraw electrons from its surface. Because $NiFe_2O_4$ is a *p*-type semiconductor, the adsorption of oxygen results in the increase in the hole density on the surface of materials and thus forms an accumulation conduction layer on its surface. Under the measured temperatures (250 °C), the adsorbed oxygen is mainly in the form of O^-, therefore, when exposed to hydrogen, the H_2 molecules interact with pre-adsorbed oxygen and release free electrons to the crystal as depicted in Eq. (6). In turn, such released electrons neutralize the holes in $NiFe_2O_4$ (Eq. (7)) result in a decrease of the total hole carriers in $NiFe_2O_4$, and consequently, an increase in the sensor resistance [30].

$$O_{2(gas)} \leftrightarrow O_{2(absorb)} \quad (2)$$

$$O_{2(abrorb)} + e^- \leftrightarrow O_2^-{}_{(absorb)} \quad (3)$$

$$O_2^-{}_{(abrorb)} + e^- \leftrightarrow 2O_2^-{}_{(absorb)} \quad (4)$$

$$O_{2\,(abrorb)} + e^- \leftrightarrow 2O^{2-}{}_{(absorb)} \quad (5)$$

$$H_{2\,(abrorb)} + O^- \leftrightarrow H_2O_{(gas)} + e^- \quad (6)$$

$$e^- + h^+ \leftrightarrow \text{null} \quad (7)$$

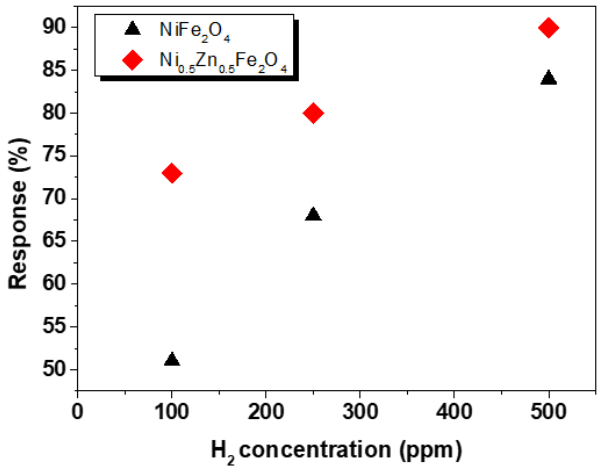

Figure 5. Response behavior of $NiFe_2O_4$ and $Ni_{0.5}Zn_{0.5}Fe_2O_4$ for different H_2 concentrations at 250 °C.

The dependence of the H_2 sensor response of $NiFe_2O_4$ and $Ni_{0.5}Zn_{0.5}Fe_2O_4$ samples in a concentration ranging from 100 ppm to 500 ppm is shown in Fig. 5. Comparing to $NiFe_2O_4$, the sensor response of $Ni_{0.5}Zn_{0.5}Fe_2O_4$ was much larger at a given concentration. For instance, at a measured H_2 concentration of 500 ppm, the sensor response of the $Ni_{0.5}Zn_{0.5}Fe_2O_4$ sample was 90%, approximately 6% larger than that of the $NiFe_2O_4$ sample (84%). The enhancement of the hydrogen sensing of Zn doped sample can be explained due to the catalytic properties of ion Zn^{2+} accelerating the interaction between H_2 molecules

and pre-adsorbed oxygen. The sensor response of both samples increased nearly linearly with increasing H_2 concentration in the measured range. The linear dependence of the sensor response on gas concentration can be explained by the dynamic equilibrium of gas adsorption and desorption during the sensing measurements, in which the number of sensing sites for H_2 adsorption is determined only by the statistical hits on the Zn surface [31]. On the other hand, by substitution of Zn^{2+} with Ni^{2+} and due to the low zinc miss the hole concentration decreases and only a small number of free electrons could be formed leading to an increase of resistivity for the synthesized samples. Obtained DC resistivity values correlate with activation energy for charge hopping between two ions calculated from plots R_a/R_g versus as shown in Fig. 4. It was observed that the band gap increases with the increase of Zn concentration in Ni–Zn ferrite [32].

4. Conclusions

$NiFe_2O_4$ and $Ni_{0.5}Zn_{0.5}Fe_2O_4$ ferrite nanoparticles were fabricated by co-precipitation combined with annealing at 800 °C. The fabricated samples were of a completely single phase of the cubic crystalline structure. The particle sizes observed from TEM images show a distribution range from 25 to 50 nm. According to Rietveld calculations, Ni^{2+} ions have been occupied in sublattice octahedral (B - site) and Zn^{2+} ions have occupied sublattice tetrahedral (A- site). The results of measuring hydrogen sensitivity with concentrations of 100 ppm - 500 ppm at 250 °C showed that the H_2 gas-sensitive response increased as the Zn doping concentration increased. Specifically, the Zn = 0.5 doped sample showed a sensitivity of 90% vs. 84% and 73% vs. 51% at concentrations of 500 ppm and 100 ppm, respectively.

Acknowledgments

This work was financially supported by the Ministry of Education and Training under Grant No. B2021-BKA-04.

References

[1] M. A. Njoroge, N. M. Kirimi, K. P. Kuria, Spinel Ferrites Gas Sensors: A Review of Sensing Parameters, Mechanism and The Effects of Ion Substitution, Critical Reviews in Solid State and Materials Sciences, Vol. 47, No. 6, 2022, pp. 807-836, https//doi.org/10.1080/10408436.2021.1935213.

[2] K. Wu, J. Li, C. Zhang, Zinc Ferrite Based Gas Sensors: A Review, Ceramics International, Vol. 45, No. 9, 2019, pp. 11143-11157, https//doi.org/10.1016/j.ceramint.2019.03.086.

[3] R. M. Shedam, P. P. Kashid, S. N. Mathad, R. B. Deshmukh, M. R. Shedam, A. B. Gadkari, Ferrites Gas Sensors: A Review, Physics and Chemistry of Solid State, Vol. 23, No. 3, 2022, pp. 626-640, https//doi.org/10.15330/pcss.23.3.626-640.

[4] A. Šutka, K. A. Gross, Spinel Ferrite Oxide Semiconductor Gas Sensors, Sensors and Actuators B: Chemical, Vol. 222, 2016, pp. 95-105, https//doi.org/10.1016/j.snb.2015.08.027.

[5] N. Rezlescu, C. Doroftei, E. Rezlescu, P. D. Popa, Lithium Ferrite for Gas Sensing Applications, Sens Actuators B Chem, Vol. 133, No. 2, 2008, pp. 420-425, https//doi.org/10.1016/j.snb.2008.02.047.

[6] A. Jain, R. K. Baranwal, A. Bharti, Z. Vakil, C. S. Prajapati, Study of Zn-Cu Ferrite Nanoparticles for LPG Sensing', The Scientific World Journal, Vol. 2013, 2013, https//doi.org/10.1155/2013/790359.

[7] P. T. T. Hoa, N. P. Duong, T. T. Loan, L. N. Anh, N. M. Hong, Gas Sensing Properties of $CuFe_2O_4$ Nanoparticles Prepared by Spray Co-Precipitation Method , Vietnam Journal of Chemistry, Vol. 57, No. 1, 2019, pp. 32-38, https//doi.org/10.1002/vjch.201960005.

[8] P. P. Hankare, S. D. Jadhav, U. B. Sankpal, R. P. Patil, R. Sasikala, I. S. Mulla, Gas Sensing Properties of Magnesium Ferrite Prepared by Co-Precipitation Method, J Alloys Compd, Vol. 488, No. 1, 2009, pp. 270-272, https//doi.org/10.1016/j.jallcom.2009.08.103.

[9] A. M. Soleimanpour, S. V. Khare, A. H. Jayatissa, Enhancement of Hydrogen Gas Sensing of Nanocrystalline Nickel Oxide by Pulsed-Laser Irradiation, ACS Appl Mater Interfaces, Vol. 4, No. 9, 2012, pp. 4651-4657, https//doi.org/10.1021/am301024a.

[10] N. Janudin et al., Polymers (Basel), Fabrication of a Nickel Ferrite/Nanocellulose-Based Nanocomposite as an Active Sensing Material for the Detection of Chlorine Gas, Polymers (Basel), Vol. 14, No. 9, 2022, https//doi.org/10.3390/polym14091906.

[11] S. Joshi, V. B. Kamble, M. Kumar, A. M. Umarji, G. Srivastava, Nickel Substitution Induced Effects on Gas Sensing Properties of Cobalt Ferrite Nanoparticles, J Alloys Compd, Vol. 654, 2016, pp. 460-466, https//doi.org/10.1016/j.jallcom.2015.09.119.

[12] C. Mukherjee, D. Mondal, M. Sarkar, J. Das, Nanocrystalline Nickel Zinc Ferrite As an Efficient Alcohol Sensor at Room Temperature, International Journal of Environment, Agriculture and Biotechnology, Vol. 2, No. 2, 2017, pp. 799-804, https//doi.org/10.22161/ijeab/2.2.29.

[13] S. Rane, M. Shinde, S. Arbuj, S. Rane, S. Gosavi, Hydrogen and Ammonia Gas Sensing Properties of Nanostructured Cobalt Doped Tin Dioxide Based Thick Films at or Near Room Temperature, Stechnolock Arch Mater Sci, 2022, pp. 1-17.

[14] N. G. Yadav, L. S. Chaudhary, P. A. Sakhare, T. D. Dongale, P. S. Patil, A. D. Sheikh, Impact of Collected Sunlight on $ZnFe_2O_4$ Nanoparticles for Photocatalytic Application, J Colloid Interface Sci, Vol. 527, 2018, pp. 289-297, https//doi.org/10.1016/j.jcis.2018.05.051.

[15] A. Pathania, P. Thakur, A. V. Trukhanov, S. V. Trukhanov, L. V. Panina, U. Lüders, A. Thakur, Development of Tungsten Doped Ni-Zn Nano-Ferrites with Fast Response and Recovery Time for Hydrogen Gas Sensing Application, Results Phys, Vol. 15, 2019, pp. 102531, https//doi.org/10.1016/j.rinp.2019.102531.

[16] A. Pathania, P. Thakur, A. Sharma, J. H. Hsu, A. Thakur, Investigation of Iron Deficient and Manganese Doped Ni–Mg Nano-Ferroxide Ceramics, Ceram Int, Vol. 41, No. 9, 2015, pp. 10803-10809, https//doi.org/10.1016/j.ceramint.2015.05.019.

[17] N. Iftimie, E. Rezlescu, P. D. Popa, N. Rezlescu, Gas Sensitivity of Nanocrystalline Nickel Ferrite, Journal of Optoelectronics and Advance Materials, Vol. 8, No. 3, 2006, pp. 1016-1018, https//doi.org/10.1127/TNO.2020.336.

[18] K. T. K. Hiratsuka, N. Muraishi, Gas Sensing Characteristics of Porous Nickel Ferrite Added with Rare Earth Metal Oxides, in 16th Chem. Sens. Symp, 1993, pp. 907.

[19] L. Satyanarayana, K. M. Reddy, S. V. Manorama, Nanosized Spinel $NiFe_2O_4$: A Novel Material for The Detection of Liquefied Petroleum Gas in Air, Mater Chem Phys, Vol. 82, No. 1, 2003, pp. 21-26, https//doi.org/10.1016/S0254-0584(03)00170-6.

[20] K. M. Reddy, L. Satyanarayana, S. V. Manorama, R. D. K. Misra, A Comparative Study of The Gas Sensing Behavior of Nanostructured Nickel Ferrite Synthesized by Hydrothermal and Reverse Micelle Techniques, Mater Res Bull, Vol. 39, No. 10, 2004, pp. 1491-1498, https//doi.org/10.1016/j.materresbull.2004.04.022.

[21] N. Rezlescu, N. Iftimie, E. Rezlescu, C. Doroftei, P. D. Popa, Semiconducting Gas Sensor for Acetone Based on the Fine Grained Nickel Ferrite, Sens Actuators B Chem, Vol. 114, No. 1, 2006, pp. 427-432, https//doi.org/10.1016/j.snb.2005.05.030.

[22] P. Ghosh, A. Mukherjee, M. Fu, S. Chattopadhya, P. Mitra, Influence of Particle size on H_2 and H_2S Sensing Characteristics of Nanocrystalline Nickel Ferrite, Physica E Low Dimens Syst Nanostruct, Vol. 74, 2015, pp. 570-575, https//doi.org/10.1016/j.physe.2015.08.023.

[23] L. N. Anh, T. T. Loan, N. K. Thanh, N. P. Duong, D. T. T. Nguyet, N. M. Hong, Structural and H_2S Sensing Properties of Copper Ferrite Nanoparticles Prepared Through Hydrothermal Method, Journal of Nanoscience and Nanotechnology, Vol. 2, No. 4, 2021, pp. 2641-2646, https://doi.org/10.1166/jnn.2021.19095.

[24] L. V. Thong, L. T. N. Loan, N. V. Hieu, Comparative Study of Gas Sensor Performance of SnO_2 Nanowires and Their Hierarchical Nanostructures, Sens Actuators B Chem, Vol. 150, No. 1, 2010, pp. 112-119, https//doi.org/10.1016/j.snb.2010.07.033.

[25] L. N. Anh, T. T. Loan, N. P. Duong, D. T. T. Nguyet, T. D. Hien, Single Phase Formation, Cation Distribution, and Magnetic Characterization of Coprecipitated Nickel-Zinc Ferrites, Anal Lett, Vol. 48, No. 12, 2015, pp. 1965-1978, https//doi.org/10.1080/00032719.2014.1003430.

[26] R. D. Shannon, Revised Effective Ionic Radii and Systematic Studies of Interatomic Distances in Halides and Chalcogenides, Acta Crystallographica Section A, Vol. 32, No. 5, 1976, pp. 751-767, https//doi.org/10.1107/s0567739476001551.

[27] I. H. Kadhim, H. A. Hassan, Q. N. Abdullah, Hydrogen Gas Sensor Based on Nanocrystalline SnO_2 Thin Film Grown on Bare Si Substrates, Nanomicro Lett, Vol. 8, No. 1, 2016, pp. 20-28, https//doi.org/10.1007/s40820-015-0057-1.

[28] S. Dhall, K. Sood, R. Nathawat, Room Temperature Hydrogen Gas Sensors of Functionalized Carbon Nanotubes Based Hybrid Nanostructure: Role of Pt Sputtered Nanoparticles, Int J Hydrogen Energy, Vol. 42, No. 12, 2017, pp. 8392-8398, https//doi.org/10.1016/j.ijhydene.2017.02.005.

[29] T. Hübert, L. B. Brett, G. Black, U. Banach, Hydrogen Sensors - A Review, Sensors and Actuators, B: Chemical, Vol. 157, No. 2, 2011, pp. 329-352, https//doi.org/10.1016/j.snb.2011.04.070.

[30] N. D. Hoa, P. V. Tong, C. M. Hung, N. V. Duy, N. V. Hieu, Urea Mediated Synthesis of $Ni(OH)_2$ Nanowires and Their Conversion Into NiO Nanostructure for Hydrogen Gas-Sensing Application, Int J Hydrogen Energy, Vol. 43, No. 19, 2018, pp. 9446-9453, https//doi.org/10.1016/j.ijhydene.2018.03.166.

[31] N. V. Duy, N. D. Hoa, N. V. Hieu, Effective Hydrogen Gas Nanosensor Based on Bead-Like Nanowires of Platinum-Decorated Tin Oxide, Sens Actuators B Chem, Vol. 173, 2012, pp. 211-217, https//doi.org/ 10.1016/j.snb.2012.06.079.

[32] G. P. Joshi, N. S. Saxena, R. Mangal, A. Mishra, T. P. Sharma, Band Gap Determination of Ni-Zn Ferrites, Bulletin of Materials Science, Vol. 26, 2003, pp. 387-389, https//doi.org/10.1007/BF02711181.